

Phase diagram of a d -wave superconductor with Anderson impurities

L. S. Borkowski

Faculty of Physics, Adam Mickiewicz University, Umultowska 85, 61-614 Poznan, Poland

We present a self-consistent solution for a model of a d -wave superconductor with finite concentration of Anderson impurities at zero temperature using the slave boson method. We show how the phase diagram depends on the strength of interaction between impurity and extended states. For fixed impurity level energy E_0 in the Kondo limit there is one superconducting-normal state transition for all impurity concentrations n . When E_0 is close the Fermi energy there are three such transitions for impurity concentration exceeding certain minimum value $n(\Gamma_0, E_0)$. If hybridization Γ_0 is fixed and the depth of the impurity level is varied, there are always two transitions for concentration above $n(\Gamma_0, E_0)$.

The problem of magnetic and nonmagnetic impurities in superconductors (SC) has a long history. Recent years brought new experimental results, most of which concern strongly correlated systems such as high-temperature and heavy-fermion superconductors.¹ Many of these studies are complicated by the uncertainty about the symmetry of the order parameter in various compounds as well as the precise nature of the interaction between localized and extended states. The proximity to antiferromagnetism in many of these materials poses additional challenges.

Scanning tunneling microscopy experiments in $\text{Bi}_2\text{Sr}_2\text{CaCu}_2\text{O}_{8+\delta}$ reveal inhomogeneities on a nanoscopic scale.²⁻⁶ Local variations of chemical composition, e.g. presence of excess oxygen atoms and cationic disorder outside the CuO_2 planes might be responsible for these modulations of the local gap and local density of states (DOS). In bismuth strontium copper oxide (BSCCO) doped with magnetic impurity Ni resonances in local density of states attributed to impurity were observed only in small-gap domains and no such resonances were seen in large-gap regions.⁵ This sensitivity of local DOS to the size of the gap may result from the proximity to the critical point where magnetic impurities become decoupled from the superconductor.⁷⁻¹⁰

Motivated by these works we will try to understand how the phase diagram of a superconductor with magnetic impurities depends on the position of the impurity level, the strength of interaction between localized state and conduction electrons and the impurity concentration. By changing the depth of the impurity level we can switch from the Kondo limit to the mixed valence regime. The phase diagram in these two cases is qualitatively different. Knowing the general form of the phase diagram may improve our understanding of experiments in impurity-doped superconductors.

I. MODEL

The model consists of electrons in a conduction band with BCS-type pairing interacting with Anderson impurity,

$$H = \sum_{k,m} \epsilon_k c_{km}^\dagger c_{km} + E_0 \sum_m f_m^\dagger f_m + V \sum_{k,m} [c_{k,m}^\dagger f_m b + H.c.] + \sum_{k,m} [\Delta(k) c_{km}^\dagger c_{-k-m}^\dagger + H.c.]. \quad (1)$$

The operator c_{km}^\dagger creates electron in a spin-orbit partial wave state of angular momentum m and momentum k . The energies ϵ_k lie in a band of half-width D and constant density of states $N_0 = 1/2D$. The impurity state has energy E_0 and its hybridization matrix element with extended states is V . The constraint $n_f + b^\dagger b = 1$ is added to prevent double occupancy of the impurity site.

We assume a two-dimensional d -wave order parameter of the form $\Delta(k) = \Delta_0 \cos(2\phi)$, where ϕ is the angle in the $k_x - k_y$ plane. In the mean field approximation the dynamics of the boson fields is neglected and the boson fields are replaced by their expectation values $\langle b^\dagger \rangle = \langle b \rangle = z^{1/2}$. Minimizing the free energy with respect to the auxiliary boson field and position of the many-body resonance ϵ_f we arrive at the mean field equations

$$\frac{1}{N} = -\text{Im} \int_{-\infty}^{\infty} d\omega f(\omega) \frac{1}{2} \text{Tr}(\tau_0 + \tau_3) \mathbf{G}_f(\omega + i0^+) \quad , \quad (2)$$

$$\frac{E_0 - \epsilon_f}{V^2} = \text{Im} \int_{-\infty}^{\infty} d\omega f(\omega) \frac{1}{2} \text{Tr}[(\tau_0 + \tau_3) \times \mathbf{G}^0(\omega + i0^+) \mathbf{G}_f(\omega + i0^+)] \quad , \quad (3)$$

where the conduction electron Green's function in clean superconductor \mathbf{G}^0 is given by

$$(\mathbf{G}^0(\omega))^{-1} = \omega\tau_0 - \epsilon_k\tau_3 - \Delta(k)(\tau_1 - i\tau_2) \quad , \quad (4)$$

and the full impurity Green's function is

$$\mathbf{G}_f^{-1}(\omega) = \omega\tau_0 - \epsilon_f\tau_3 - \Sigma_f(\omega) \quad . \quad (5)$$

Conduction electron Green's function is averaged over impurity positions in the usual way. We have to solve

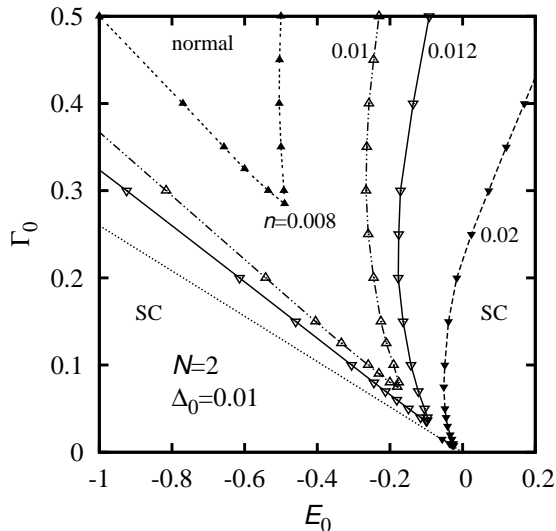


FIG. 1: The phase diagram of d -wave superconductor with Anderson impurities for four values of impurity concentration. The lines separate the normal state from the superconductor (SC). The broken line shows location of the impurity quantum phase transition. Below that line the impurities are decoupled from the superconductor. The slope of this line is approximately -0.26 which agrees with the numerical renormalization group⁹ result and a single-impurity large- N calculation for a d -wave superconductor.¹¹

the system of equations (2), (3), together with the gap equation

$$\Delta(k) = \int_{-\infty}^{\infty} d\omega f(\omega) \sum_{k'} V_{kk'} \text{Tr} \frac{1}{2} (\tau_1 - i\tau_2) \mathbf{G}(k', \omega). \quad (6)$$

For each frequency ω we solve self-consistently the Dyson equations for conduction electron and impurity self-energies

$$\Sigma(\omega) = \mathbf{G}^0(\omega) - \frac{nN}{2\pi N_0} \Gamma \mathbf{G}_f(\omega), \quad (7)$$

$$\Sigma_f(\omega) = \mathbf{G}_f^0(\omega) - \Gamma \sum_k \mathbf{G}(k, \omega), \quad (8)$$

where n is the concentration of impurities, N is the degeneracy of the impurity energy level E_0 , $\Gamma = z\Gamma_0 = z\pi N_0 V^2$. Here we assumed $N = 2$.

The self-energy $\Sigma_f(\omega)$ in eqn. (5) in general contains both diagonal and off-diagonal terms in particle-hole space. Here the off-diagonal term is zero due to vanishing of the Fermi surface average of the off-diagonal part of the conduction electron Green's function.

The renormalized frequencies are solutions of the following equations

$$\tilde{\omega} = \omega + \Gamma \left\langle \frac{\tilde{\omega}}{(\Delta^2(k) - \tilde{\omega}^2)^{1/2}} \right\rangle, \quad (9)$$

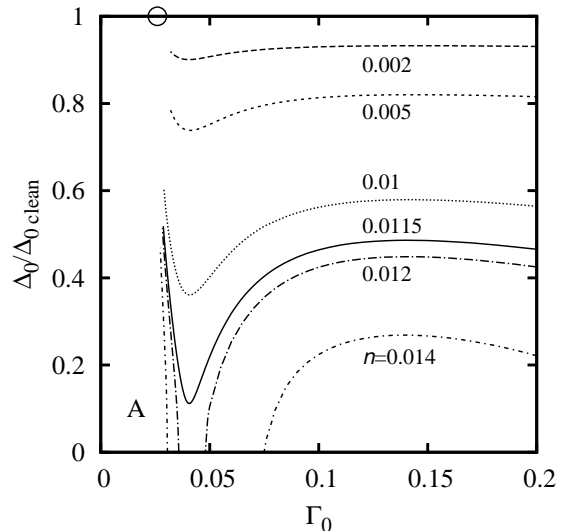


FIG. 2: The amplitude of the order parameter as a function of bare hybridization Γ_0 for $E_0 = -0.1$ and several impurity concentrations. The approximate location of the critical point where impurities are decoupled from the conduction band is marked with a circle.

and

$$\tilde{\omega} = \omega + \frac{nN}{2\pi N_0} \frac{\bar{\omega}}{(-\bar{\omega}^2 + \epsilon_f^2)}. \quad (10)$$

where brackets denote average over the Fermi surface. The presence of full Green's functions under integrals of eqs. (3), (4) and (7) means eqs. (10) and (11) have to be solved at each step in the integration routines.

II. RESULTS

The calculations were performed for nondegenerate impurities, $N = 2$, with superconducting order parameter $\Delta_0 = 0.01$. All energies are given in units of D .

The obtained phase diagram is shown in Fig. 1. In the Kondo limit the superconducting-normal state boundary is a straight line. In the mixed valence regime the boundary for fixed E_0 is nonmonotonic.

Fig. 2 shows Δ_0 as a function of Γ_0 for $E_0 = -0.1$. There is a local gap minimum at intermediate values of Γ_0 , where $T_K \sim T_{c0}$, where T_K is defined as $\sqrt{\Gamma^2 + \epsilon_f^2}$. Pair breaking is strongest when the two energy scales are comparable. For $n \gtrsim 0.0117$ there appears a normal state around $\Gamma_{0c} \simeq 0.04$. For $\Gamma_0 < \Gamma_{0c}$, in the region marked "A" in Fig. 2 the order parameter quickly rises to the value of the clean limit. Here the system is very sensitive to details of interaction. The steep curve at the boundary of region A means that small change of Γ_0 or impurity concentration may completely alter system properties. The normal state is separated from the clean-like superconductor by only about 10% change of Γ_0 . Experiments conducted in this regime may be subject to

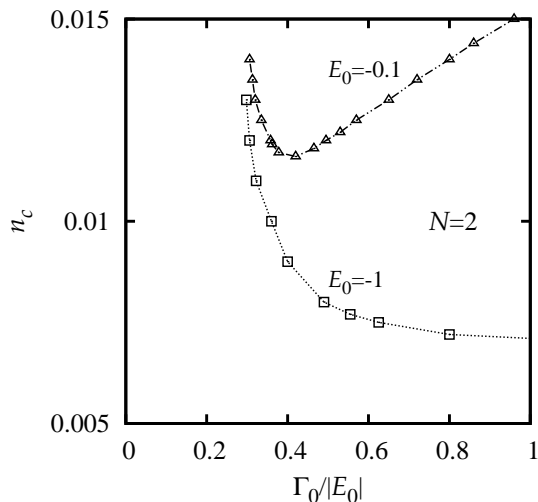


FIG. 3: Critical concentration for the superconducting-normal transition as a function of $\Gamma_0 = \pi N_0 V^2$ for $E_0 = -1$ and $E_0 = -0.1$. The $E_0 = -1$ curve shows the behavior in the Kondo limit.

greater errors than that in other parts of the phase diagram. Also the presence of local disorder around each impurity significantly influences the system behavior in this limit. Inhomogeneities in experimental samples, whether intrinsic to the superconducting state or influenced by impurity doping, may lead to situation where the system is normal in some regions and superconducting in the rest of the sample.

For $\Gamma_0 > \Gamma_{0c}$ the impurity resonance widens and pair breaking at low energies is less effective. Further increase of Γ_0 raises pair-breaking for all energies and eventually the normal state becomes more stable. Numerical difficulties prevent us from finding the exact location of the point where $\Delta_0/\Delta_{0 \text{ clean}} \rightarrow 1$. However this is not necessary for the purpose of this paper. We can see in Figs. 3 and 4 that decoupling of impurities from the conduction band occurs at the same critical value of Γ_0/E_0 for different choices of E_0 .

The phase diagram in the n vs. $\Gamma_0/|E_0|$ plane is shown in Fig. 2. In the well developed Kondo limit, when the bare impurity energy level E_0 is deep below the Fermi surface and impurity occupation number $n_f \simeq 1$, there is only one superconducting-normal transition. This is illustrated by the $E_0 = -1$ curve in Fig. 3. The transition line is monotonic in the entire phase diagram.

When E_0 lies closer to the Fermi surface, see curve $E_0 = -0.1$, there exists a critical concentration n'_c such that for $n < n'_c$ the system remains superconducting for small and moderate values of $\Gamma_0/|E_0|$ and the transition to the normal state occurs at $\Gamma_0/|E_0| \gg 1$ (beyond the range shown in Fig. 3). However for $n > n'_c$ there are two additional transitions for intermediate values of $\Gamma_0/|E_0|$, when $T_K \sim T_{c0}$.

This is clearly shown in Fig. 4 where $E_0 = -0.01$. The horizontal axis of Fig. 4 is extended to larger values of Γ_0 . This is the general form of the phase diagram when E_0

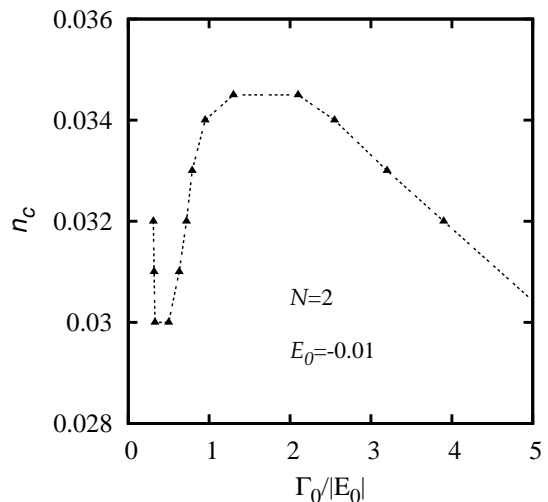


FIG. 4: The phase diagram in the mixed valence limit, $E_0 = -0.01$. The scale of the horizontal axis is changed relative to Fig. 2 to illustrate behavior at large Γ_0 .

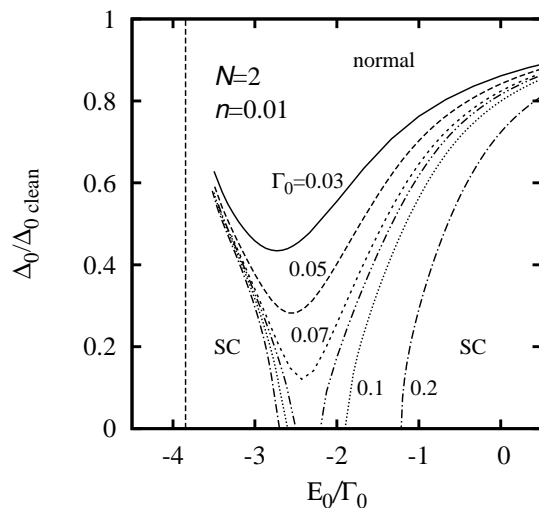


FIG. 5: Superconducting order parameter Δ_0 as a function of E_0 for several values of Γ_0 at $n = 0.01$. The unmarked dash-dotted curve is the result for $\Gamma_0 = 0.08$. The vertical dotted line marks the impurity quantum phase transition.

is close to the Fermi energy. The superconducting state boundary for $E_0 = -0.1$ has similar shape (not shown in Fig. 3 due to smaller horizontal scale). For increasing E_0 the phase transition line is shifted towards higher impurity concentrations and the normal state section at intermediate $\Gamma_0/|E_0|$ becomes narrower. This can be explained by the weaker pair breaking in the mixed valence regime.

The impurity-induced peak in the conduction electron DOS remains at $\omega = 0$ for all $E_0 < 0$. The peak splits in two, one at positive ω and one at negative ω when $\epsilon_f \gg \Gamma$. For a nondegenerate impurity in a superconductor with order parameter having lines of nodes this occurs only at $E_0 > 0$. This conclusion was verified numerically.

The dependence of the order parameter on E_0 for several values of Γ_0 is shown in Fig. 5. This behavior is always nonmonotonic. The minimum Δ_0 occurs when $T_K \sim \Delta_0$. For larger Γ_0 we have two superconducting regions, one in the Kondo limit and one in the mixed valence regime, separated by the normal state.

III. CONCLUSIONS

The impurity quantum phase transition at finite coupling is associated with the particle-hole asymmetry of the model.⁹ If the impurity degeneracy N is increased, the impurity transition occurs at lower coupling.¹² This is expected since for larger N the impurity resonance is located at higher energy. The precise location of the main features of the phase diagram changes but its overall qualitative form remains intact.¹²

The suppression of the superconducting state along the diagonal of the phase diagram in Fig. 1 results from the interplay of energy scales and is not directly related to the symmetry of the order parameter. In an s-wave superconductor the steepest initial decrease of the superconducting critical temperature as a function of impurity concentration, $(dT_c/dn)|_{T_c=T_{c0}}$ occurs for $T_{c0} \sim T_K$.¹³ At $T = 0$ this corresponds to $\Delta_0 \sim T_K$ and we expect a normal state insertion similar to that in Fig. 1 also for order parameters without nodes on the Fermi surface.

Features of the phase diagram should be visible in experiments by (a) changing impurity concentration at fixed carrier doping and (b) varying the strength of coupling to the impurity, the ratio Γ_0/E_0 , at fixed impurity concentration.

The depth of the impurity level may be tuned by applying pressure. There exist studies of heavy-fermion compounds, most notably $\text{CeCu}_2(\text{Si}_{1-x}\text{Ge}_x)_2$ where varying hydrostatic pressure reveals two superconducting regions

in the phase diagram.¹⁴ The change of pressure shifts the chemical potential. Position of the bare impurity level E_0 of Ce ions relative to E_F changes accordingly. This may explain the existence of two superconducting regions in the phase diagram of $\text{CeCu}_2(\text{Si}_{1-x}\text{Ge}_x)_2$ similarly to results of this work. Increasing pressure brings the system into the mixed-valence regime. It is equivalent to increasing the ratio $\Gamma_0/|E_0|$ in our work. The existing explanation for the superconducting region at high pressure uses the concept of the valence-fluctuation mediated pairing mechanism.¹⁵ It is interesting to note that a qualitatively similar nonmonotonic behavior of superconducting critical temperature is obtained in an impurity problem when increasing E_0 . We hope that similar experiments under varying pressure may be conducted on superconductors with Anderson impurities. They should reveal the details of the phase diagram described in this article.

A nontrivial question is realistic treatment of finite impurity concentrations in this problem. In real samples there are local inhomogeneities and variations of impurity concentration. There is some evidence that inhomogeneity of the superconducting state may be intrinsic in some high- T_c compounds even in absence of impurities in CuO_2 planes.¹⁶ This may have important consequences near the transition line in the region A of the phase diagram in Fig. 2, where a small change in hybridization or impurity level E_0 implies a large change in properties. In this limit the entire sample might even consist of a mixture of normal and superconducting patches. This sensitivity should be also visible in the low-energy physics near the impurity critical point. In inhomogeneous samples pockets of clean-like superconductor may coexist with regions where low-energy physics is dominated by Kondo impurities. Scanning tunneling microscopy (STM) measurements should be helpful in investigating the phase diagram in the vicinity of the superconducting state boundary and the impurity critical point.

¹ H. Alloul, J. Bobroff, M. Gabay, and P.J. Hirschfeld, Rev. Mod. Phys. **81**, 45 (2009); A. V. Balatsky, I. Vekhter, and J.-X. Zhu, *ibid.* **78**, 373 (2006), and references therein.
² T. Cren, D. Roditchev, W. Sacks, J. Klein, J.-B. Moussy, C. Deville-Cavellin, and M. Lagues, Phys. Rev. Lett. **84**, 147 (2000).
³ S.-H. Pan, J. P. O'Neal, R. L. Badzey, C. Chamon, H. Ding, J. R. Engelbrecht, Z. Wang, H. Eisaki, S. Uchida, A. K. Guptak, K. Ng, E. W. Hudson, K. M. Lang, and J. C. Davis, Nature **413**, 282 (2001).
⁴ C. Howald, P. Fournier, and A. Kapitulnik, Phys. Rev. B **64**, 100504(R) (2001).
⁵ K. M. Lang, V. Madhavan, J. E. Hoffman, E. W. Hudson, H. Eisaki, S. Uchida, and J. C. Davis, Nature **415**, 412 (2002).
⁶ K. McElroy, J. Lee, J. A. Slezak, D.-H. Lee, H. Eisaki, S. Uchida, and J. C. Davis, Science **309**, 1048 (2005).
⁷ D. Withoff and E. Fradkin, Phys. Rev. Lett. **64**, 1835 (1990).

⁸ L.S. Borkowski and P.J. Hirschfeld, Phys. Rev. B **46**, 9274, 1992.
⁹ C. Gonzalez-Buxton and K. Ingersent, Phys. Rev. B **57**, 14254 (1998).
¹⁰ M. Vojta, Rep. Prog. Phys. **66**, 2069 (2003).
¹¹ G.-M. Zhang, H. Hu, and L. Yu, Phys. Rev. B **66**, 104511 (2002).
¹² L. S. Borkowski, unpublished.
¹³ N. E. Bickers and G. E. Zwicknagl, Phys. Rev. B **36**, 6746 (1987), L. S. Borkowski and P. J. Hirschfeld, J. Low Temp. Phys., **96**, 185 (1994), and references therein.
¹⁴ H. Q. Yuan, F. M. Grosche, M. Deppe, C. Geibel, G. Sparn, and F. Steglich, New J. Phys. **6**, 132 (2004), P. Gegenwart, Q. Si, F. Steglich, Nature Physics, **4**, 186 (2008).
¹⁵ K. Miyake and H. Maebashi, J. Phys. Soc. Japan **71**, 1007 (2002).
¹⁶ Y. He, S. Graser, P. J. Hirschfeld, and H.-P. Cheng, Phys. Rev. B **77**, 220507 (2008).